

See discussions, stats, and author profiles for this publication at: <https://www.researchgate.net/publication/223366082>

The formation and evolution of the barrier islands of Inhaca and Bazaruto, Mozambique

Article in *Geomorphology* · December 2006

DOI: 10.1016/j.geomorph.2006.05.011

CITATIONS

40

READS

92

6 authors, including:



[Simon James Armitage](#)

Royal Holloway, University of London

54 PUBLICATIONS 1,835 CITATIONS

[SEE PROFILE](#)



[Gregory A. Botha](#)

Council for Geoscience

49 PUBLICATIONS 746 CITATIONS

[SEE PROFILE](#)



[Geoff Duller](#)

Aberystwyth University

195 PUBLICATIONS 9,087 CITATIONS

[SEE PROFILE](#)

Some of the authors of this publication are also working on these related projects:



Briquetage de la Seille [View project](#)



BRITICE-CHRONO [View project](#)

All content following this page was uploaded by [Gregory A. Botha](#) on 11 April 2016.

The user has requested enhancement of the downloaded file. All in-text references [underlined in blue](#) are added to the original document and are linked to publications on ResearchGate, letting you access and read them immediately.

The formation and evolution of the barrier islands of Inhaca and Bazaruto, Mozambique

S.J. Armitage^{a,b,*}, G.A. Botha^c, G.A.T. Duller^b, A.G. Wintle^b,
L.P. Rebêlo^d, F.J. Momade^e

^a Oxford University Centre for the Environment, Dyson Perrins Building, South Parks Road, Oxford, OX1 3QY, United Kingdom

^b Institute of Geography and Earth Sciences, University of Wales, Aberystwyth, Ceredigion, SY23 3DB, United Kingdom

^c Council for Geoscience, KwaZulu-Natal Unit, P.O. Box, Pietermaritzburg, 3220, South Africa

^d Instituto Geológico e Mineiro, Departamento de Geologia Marinha, Estrada da Portela, Zambujal, Apartado 7586,
2721-866 Alfragide, Portugal

^e Direção Nacional de Geologia, P.O. Box 217, Maputo, Mozambique

Received 19 October 2005; received in revised form 17 May 2006; accepted 17 May 2006

Available online 7 July 2006

Abstract

The barrier islands of Inhaca and Bazaruto are related to the extensive coastal dune system of the Mozambican coastal plain, south-east Africa. Optically stimulated luminescence (OSL) dating of key stratigraphic units indicates that accretion of sediment within these systems is episodic. Both islands appear to have been initiated as spits extending from structural offsets in the coastline. Superposition of significant quantities of sediment upon these spits during subsequent sea-level highstands formed the core of the islands, which were anchored and protected by beachrock and aeolianite formation. At least two distinct dune-building phases occurred during Marine Oxygen Isotope Stage (MIS) 5, tentatively attributed to marine transgressions during sub-stages 5e and 5c. Although some localized reactivation of dune surfaces occurred prior to the Holocene, large quantities of sediment were not deposited on either island during the low sea-levels associated with MIS 2. Significant dune-building and sediment reworking occurred immediately prior to and during the Holocene, though it is not clear whether these processes were continuous or episodic. Significant erosion of the eastern shoreline of Bazaruto suggests that it is far less stable than Inhaca and may suffer further large-scale erosion. A model is presented for the formation of barrier islands along the Mozambican coastal plain.

© 2006 Elsevier B.V. All rights reserved.

Keywords: Coastal evolution; Barrier islands; Inhaca; Bazaruto; Mozambique; OSL

1. Introduction

Along the south-east coast of Africa, there is a continuous coastal plain that runs from Durban in the

Republic of South Africa to Beira in Mozambique. The Mozambican coastal plain is up to 440 km wide south of the Save River, narrowing southward towards the Maputaland coastal plain, south of Maputo (Fig. 1). Extensive coastal dune systems of Neogene to recent age characterize the coastal zone which is dominated by a composite accretionary coastal barrier dune cordon, containing some of the highest coastal dunes in the world (Cooper and Pilkey, 2002; Botha et al., 2003).

* Corresponding author. Oxford University Centre for the Environment, Dyson Perrins Building, South Parks Road, Oxford, OX1 3QY, United Kingdom. Tel.: +44 1865 285086.

E-mail address: simon.armitage@ouce.ox.ac.uk (S.J. Armitage).

Inland of this dune cordon are extended parabolic, sinuous crested and hummocky dunes. Due to the dune sand cover and absence of natural exposures or sections that display the stratigraphic relationships between dune sand bodies, the age relationships between these aeolian deposits have only recently begun to be understood. Extensive field investigation and geological mapping of the Maputaland coastal plain in South Africa, combined with ground penetrating radar and infrared stimulated luminescence dating studies (Botha and Porat, 2000; Botha et al., 2003), have revealed a history of aeolian deposition and polyphase reworking during the Pleistocene and Holocene. These processes have yielded a complex and dynamic coastal dune system for which the regional lithostratigraphic framework has been described by Maud and Botha (2000). Additional geochronological detail regarding the accretion of the coastal barrier dune and closure of coastal lakes and estuaries during the mid-Holocene has been derived from radiocarbon dating of beachrocks, lacustrine infill deposits and marine shells in southern Maputaland (Ramsay, 1995; Wright et al., 2000; Miller, 2001; Wright, 2002; Ramsay and Cooper, 2002).

Inhaca and Bazaruto are barrier islands within the relatively unstudied Mozambican portion of the coastal plain (Fig. 1). The regional geology reflects late Jurassic volcanism followed by marine inundation since the lower Cretaceous, during which time the region south of the Save River was a major depocentre (Flores, 1973). Bedrock in the Vilanculos area consists of Neogene evaporites. Structures associated with the Urema graben, the southern extension of the African Rift, extend southwards to this area (Flores, 1973; Förster, 1975). The Maputo Bay area is underlain by Eocene and Neogene marine deposits but is less affected by tectonism (Achimo et al., 2004). Whereas the linear coastline from Inhambane to Vilanculos could reflect structural control, the location of Inhaca Island in Maputo Bay reflects a palaeotopographic influence during the marine transgressions and regressions of the Pleistocene. Cooper and Pilkey (2002) regarded these islands as having formed as spits generated at structural offsets in the coastline, close to the break of slope of the continental shelf, during a period when sea-level was as high as at the present day. Subsequent aeolian deposition raised the relief of both islands, while the cementation of aeolian deposits to form aeolianite, and beach sediments to form beachrock, served to protect them from marine erosion. Both islands face the open Indian Ocean and are backed by wide back-barrier bays characterized by extensive sub- and inter-tidal sand bars (Cooper and Pilkey, 2002).

Due to the steep, narrow continental shelf (Fig. 1), neither island was more than 5 km from the coast during the Marine Oxygen Isotope Stage (MIS) 2 low sea-level (Cooper and Pilkey, 2002).

Sediment supply is high due to the presence of several major rivers in the region and the large quantities of unconsolidated aeolian sands in the littoral zone. Coastal sediment transport by longshore currents is predominantly northwards due to the preponderance of SE Trade Winds and swell regimes (Ramsay, 1994). The Agulhas Current flows southwards off Bazaruto but forms a large eddy in Maputo Bay leading to northerly flow off Inhaca (Flemming, 1981). The mean spring tidal range is ~3 m. Both islands receive annual rainfall of ~1000 mm (Cooper and Pilkey, 2002). The compact nature of Inhaca and Bazaruto and the stratigraphic relationships revealed along the eroded coastline make these islands ideal for studying both the evolution of barrier islands and the more general geomorphic development of the south-east African coastal dune complex to which they belong.

Several studies have described the evolution and main geomorphic units of Inhaca (Hobday, 1977; Cooper and Pilkey, 2002), Bazaruto (Cooper, 1991; Cooper and Pilkey, 2002) and the south-east African coastal plain (Maud and Botha, 2000; Botha et al., 2003). However, these studies contain very few absolute ages. Optically stimulated luminescence (OSL) is the ideal dating method for these sediments, as outlined in a recent review by Duller (2004). The aim of this paper is to produce a model for the evolution of barrier islands along the Mozambique coast by using OSL to date the main geomorphic units of Inhaca and Bazaruto.

1.1. Inhaca

Inhaca consists of two distinct, north–south-oriented dune ridges (Fig. 2). The seaward ridge appears to contain an aeolianite core, which is exposed at Cabo Inhaca. This aeolianite is notched at 5–6 m above present sea-level, a feature which Hobday (1977) ascribes to the MIS 5e high sea-level event. A nearly continuous fringe of beachrock is exposed in the intertidal zone along the ocean margin of the island, and less continuously elsewhere. Both active and vegetated, NW-oriented, ascending parabolic dunes form the eastern dune cordon, attaining a maximum elevation of 120 m. The western dune cordon along the embayed Barreira Vermelha coastline (Muacanhia, 2004) of Inhaca is characterized by high bluffs that reveal a core of planar cross-bedded aeolianite overlain by a decalcified weathering profile of reddened sands. In



Fig. 1. Map showing Mozambique and the Republic of South Africa. The limit of the coastal plain is indicated broadly by the 100 m contour. The inset also shows the location of Cape Agulhas, Blombos and Wilderness which are mentioned in the text.

other locations along the bay margin, eroded sands have accumulated to form barriers and beaches hinged on beachrock and aeolianite outcrops (Cooper and Pilkey, 2002). The elevated eastern and western dune cordons are linked by a lower-lying, undulating plain where the surface morphology is dominated by the vegetation-stabilized trailing limbs of parabolic dunes. Some of these parabolic dunes are truncated at their northern end by a palaeo-tidal flat, at an elevation of 3.5 m, while others override it.

1.2. Bazaruto

Bazaruto is the most northerly and largest of four islands in the Bazaruto archipelago (Figs. 1 and 3). The central core of the north–south-oriented island is comprised of degraded Pleistocene dunes of structureless reddish yellow sand, discontinuously exposed at bluffs along the cusped bayside margin of Bazaruto. The northern part of the island preserves an extensive wetland system which possibly formed as a mangrove

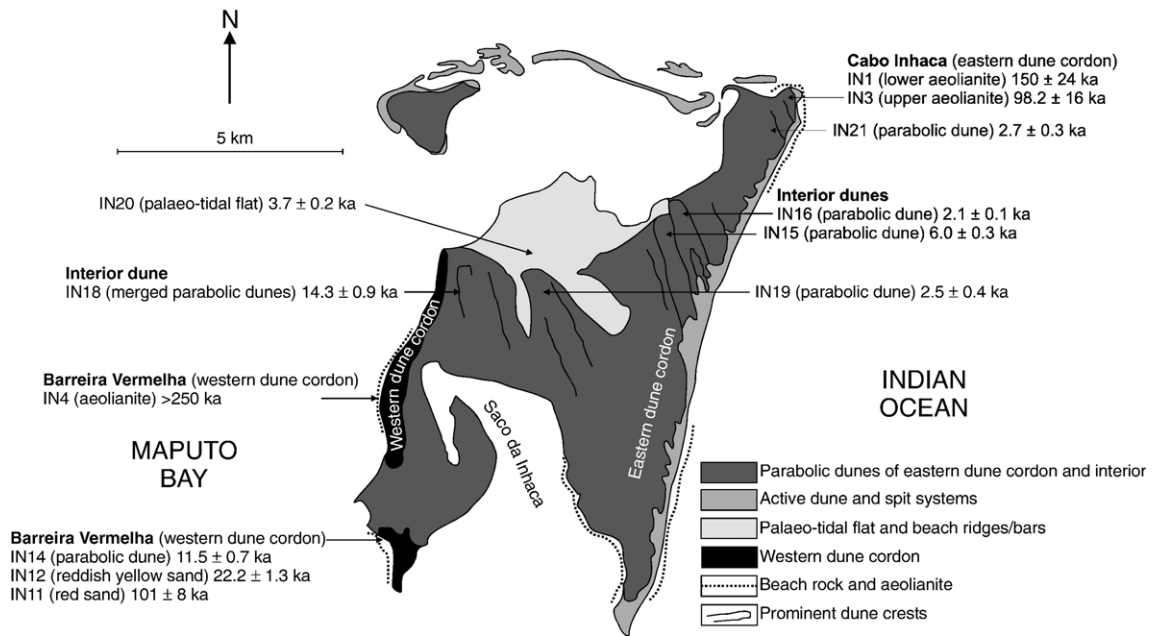


Fig. 2. Sample locations and key geomorphic features of Inhaca Island.

and salt-marsh system during a period of slightly higher mid-Holocene sea-level. Contemporary mangrove swamps and marshes are formed behind low foredune systems. Along the ocean margin and at points on the cusped back-barrier bay coastline, discontinuous outcrops of beachrock alternate with sandy beaches. Beachrock and aeolianite outcrops form prominent points at the southern end of zeta-form bays along the eastern shore. Offshore, submerged outcrops delineate previous shorelines, possibly relating to a period of stabilization in the early Holocene (Cooper, 1991) or the marine regressions during MIS 5-2. Yellowish sands form NW-oriented climbing parabolic dune complexes along the high coastal barrier cordon along much of the eastern side of the island. The prograding transverse ridge formed by closely-spaced parabolic dunes has advanced over the lower, degraded dunes and interdune lakes, forming the undulating central part of the island (Fig. 3). The alignments of both the degraded parabolic dune forms and the interdune depressions of the interior are towards the northwest, indicating the long-term aeolian sand transport vector on the island. Coastal erosion has created steep sections that reveal the older basal sands and aeolianite that locally form the core of the island. Similar relationships between dunes and coastal geomorphology occur along much of the mainland coastline between Inhambane and Bazaruto (Fig. 1). The geomorphology of Bazaruto suggests that considerable erosion of the oceanic margin and redeposition of sediment inland has occurred in the past and continues in the present.

2. Laboratory methods

Where possible, samples for dating using OSL were collected in opaque plastic tubes hammered into the face of cleaned sections or sample pits. Consolidated material was collected in blocks. In the laboratory, samples were processed under subdued red light. Sunlight-exposed material was removed and retained for dose rate measurement. Dosimetry samples were dried and milled prior to measurement. Uranium, thorium and potassium concentrations (Table 1) were calculated using thick-source alpha-counting and gas-flow Geiger-Muller beta counting (Bøtter-Jensen and Mejdahl, 1988). For all except 5 samples the Th/U ratio is between 3 and 4, the range expected for sediments derived from crustal rocks. A moisture content of $5 \pm 5\%$ was assumed for all samples except IN20, which was taken from below the modern water table. This value is based on measured (e.g. Ballarini et al., 2003; Berger et al., 2003) and assumed (e.g. Banerjee et al., 2003) moisture contents presented in recent studies of well-drained coastal and coast proximal dune deposits. For sample IN20, a saturation moisture content of $37 \pm 5\%$ was used. This saturation moisture content was calculated by Duller (1996) assuming an average sand grain density of 2.6 g/cm^3 and sediment porosity of 49% (Atkins and McBride, 1992). Beta and gamma dose rates were calculated from radioisotope and moisture contents using the conversion factors of Adamiec and Aitken (1998). The alpha irradiated rind of the quartz

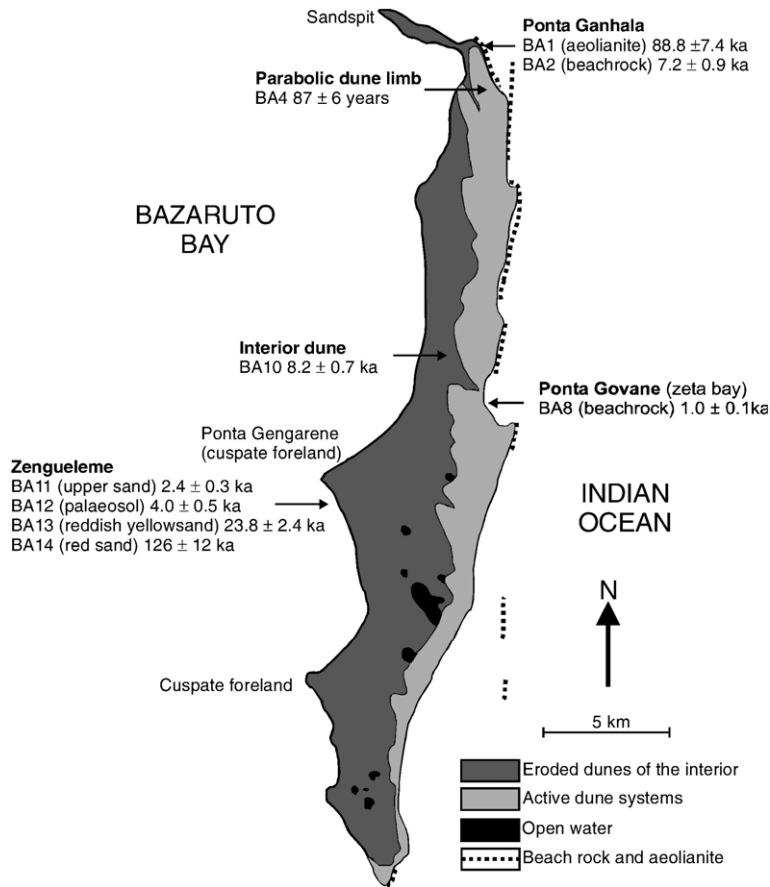


Fig. 3. Sample locations and key geomorphic features of Bazaruto Island. Detail regarding locality names was derived from the comprehensive document on the archipelago by Dutton (1990).

grains was assumed to have been removed by HF (23 M) etching for 40 min (Hong, 1998) and hence the alpha dose rate was taken to be zero. Cosmic ray dose rates were calculated using the formula given by Prescott and Hutton (1988) except where samples were buried to a depth of greater than 27 m, where the equation of Barbouti and Rastin (1983) was used. Dose rates for each sample are presented in Table 1.

For OSL dating, carbonates and organic matter were removed from the part of the sample that had not been exposed to light using 1 M HCl and 20 volumes H₂O₂. The sample was then dry sieved to 180–212 μm. Pure quartz was extracted from this fraction using density separations at 2.62 and 2.70 g/cm³ and a subsequent HF acid etch (23 M HF for 40 min followed by a 10 M HCl rinse and re-sieving). The purified quartz was held as a monolayer (2–3 mg/aliquot) on 10 mm diameter aluminium discs using Silkospray silicone oil.

The single-aliquot regenerative-dose (SAR) method (Murray and Wintle, 2000) was used to determine the equivalent dose (D_e) for each aliquot. All measurements

were carried out using one of two automated Risø TL/OSL readers, each fitted with an EMI 9635QA photomultiplier and two 3 mm thick Hoya U-340 filters. The readers were equipped with blue (470Δ20 nm) light emitting diodes (LEDs), one reader having a stimulation power of 2.2 mW/cm² and the other 16.9 mW/cm². Stimulation was carried out at 125 °C. The stimulation light was filtered using Schott GG-420 filters (Bøtter-Jensen et al., 2000). Each aliquot was stimulated for 100 s (using the 2.2 mW/cm² diodes, providing a cumulative stimulation energy of 220 mJ/cm²) or 40 s (16.9 mW/cm² diodes, providing a cumulative stimulation energy of 680 mJ/cm²). The luminescence intensity used for dating is that from the first 0.88 or 2.7 mJ/cm² of stimulation (for the 2.2 and 16.9 mW/cm² diodes, respectively) with a background signal subtracted. This background was the mean of the signal recorded in the last 10% of the OSL decay curve for both the regenerative and test dose signals. Where D_e exceeded 5 Gy, a 5 Gy test dose was used, otherwise a 1 Gy test dose was used. Aliquots were heated at 5 °C/s during all

Table 1
Summary of dosimetry and dating results

Sample	Radionuclide concentrations			Sample depth (m)	Cosmic dose rate (Gy/ka)	Dose rate (Gy/ka)	Equivalent dose, D_e (Gy)	Age (ka) ^a
	K (%)	U (ppm)	Th (ppm)					
Aber/28-IN1	0.51±0.02	0.31±0.07	0.43±0.02	3±1	0.14±0.08	0.67±0.08	101±10	150±24
Aber/28-IN3	0.81±0.03	0.35±0.05	1.46±0.17	4±2	0.13±0.14	0.98±0.14	96.2±7.1	98.2±16.0
Aber/28-IN4	0.77±0.03	0.43±0.06	1.77±0.20	30±5	0.02±0.03	0.87±0.05	>240	>250
Aber/28-IN11	1.09±0.03	0.77±0.12	3.46±0.39	40±5	0.01±0.01	1.32±0.07	133±7	101±8
Aber/28-IN12	0.78±0.02	0.37±0.05	1.50±0.17	1.4±0.2	0.18±0.02	1.01±0.05	22.4±0.9	22.2±1.3
Aber/28-IN14	1.01±0.03	0.43±0.07	2.08±0.23	1.4±0.2	0.18±0.02	1.26±0.06	14.5±0.5	11.5±0.7
Aber/28-IN15	0.64±0.02	0.33±0.04	1.11±0.13	1.5±0.2	0.17±0.02	0.86±0.04	5.2±0.2	6.0±0.3
Aber/28-IN16	0.91±0.02	0.38±0.05	1.55±0.17	1.2±0.2	0.18±0.02	1.13±0.05	2.4±0.1	2.1±0.1
Aber/28-IN18	0.63±0.02	0.44±0.04	0.81±0.12	1.2±0.2	0.18±0.02	0.85±0.04	12.2±0.5	14.3±0.9
Aber/28-IN19	0.59±0.02	0.34±0.05	1.28±0.15	1.2±0.2	0.18±0.02	0.83±0.04	2.0±0.3 (1–6) ^b	2.5±0.4 (1.2–7.2)
Aber/28-IN20	1.24±0.03	0.92±0.07	1.37±0.22	0.6±0.2	0.18±0.02	1.16±0.05	4.3±0.2	3.7±0.2
Aber/28-IN21	0.89±0.02	0.56±0.07	1.84±0.23	1.2±0.2	0.18±0.02	1.17±0.05	3.1±0.3 (1–6)	2.7±0.3 (0.9–5.1)
Aber/29-BA1	1.33±0.02	0.37±0.05	1.45±0.17	6±0.5	0.10±0.03	1.40±0.08	124±8	88.8±7.4
Aber/29-BA2	0.88±0.03	0.33±0.04	1.05±0.13	0.5±0.2	0.21±0.02	1.09±0.05	7.8±0.9	7.2±0.9
Aber/29-BA4	0.97±0.03	0.74±0.09	2.49±0.30	1.2±0.2	0.18±0.02	1.31±0.06	0.11±0.01	0.087±0.006
Aber/29-BA8	1.68±0.03	0.31±0.02	0.49±0.07	0.5±0.2	0.21±0.02	1.73±0.09	1.7±0.2 (0.5–3)	1.0±0.1 (0.3–1.7)
Aber/29-BA10	2.05±0.03	0.40±0.05	1.33±0.16	1.2±0.2	0.18±0.02	2.09±0.11	17.1±1.2 (5–25)	8.2±0.7 (2.4–12)
Aber/29-BA11	1.18±0.03	0.57±0.07	2.17±0.24	2±0.5	0.16±0.04	1.42±0.08	3.4±0.4 (0.5–8)	2.4±0.3 (0.4–5.6)
Aber/29-BA12	1.48±0.04	0.76±0.12	3.59±0.39	4±0.5	0.13±0.03	1.77±0.09	7.0±0.8 (2–14)	4.0±0.5 (1.1–7.9)
Aber/29-BA13	1.03±0.03	0.58±0.07	2.09±0.23	6±0.5	0.12±0.02 ^c	1.25±0.06	29.7±2.6	23.8±2.4
Aber/29-BA14	1.30±0.02	0.50±0.05	1.09±0.15	20±2	0.12±0.02	1.39±0.07	176±14	126±12

^a Uncertainties are based on the propagation, in quadrature, of errors associated with individual errors for all measured quantities. In addition to uncertainties calculated from counting statistics, errors due to (1) beta source calibration (3%, [Armitage and Bailey, 2005](#)), (2) alpha and beta counter calibration (3%), (3) dose rate conversion factors (3%) and (4) attenuation factors (2%) have been included ([Murray and Olley, 2002](#)). A water content of 5±5% was used for all samples except for IN20 where 37±5% was used.

^b Figures in parentheses indicate the range from lowest to highest measured individual D_e value for samples yielding wide equivalent dose distributions (see Section 3.2). Ages in parentheses indicate the apparent age of the youngest and oldest aliquot for these samples.

^c Cosmic dose rates for BA13 and 14 were calculated in stages, to allow for accumulation of the overlying deposits ([Armitage, 2003](#)). The cosmic dose rate quoted is the mean value.

heating steps, and a 10 s pause at 125 °C prior to optical stimulation was used to allow for the lag in temperature between the thermocouple and sample. For the preheat (PH1) prior to measurement of the natural/regenerated OSL signal (L_x), a range of temperatures were used for each sample, usually with three aliquots at each temperature in the range 160–300 °C in 20 °C increments (24 aliquots per sample). A cut-heat to 160 °C (PH2) was used prior to measurements of the test dose response (T_x), irrespective of the PH1 temperature.

The luminescence properties of samples used in this study have been reported by [Armitage et al. \(2000\)](#), [Duller et al. \(2000\)](#) and [Armitage \(2003\)](#). The studies indicate that the material is sensitive to both dose and light exposure, yielding very bright OSL signals per unit dose, and that the SAR method produces reliable results when applied to these samples. Briefly, aliquots yielding recycling ratios ([Murray and Wintle, 2000](#)) or IR depletion ratios ([Duller, 2003](#)) differing from unity by greater than 10% were rejected. [Fig. 4](#) shows the recycling ratios for all 652 aliquots measured in this

study. The majority of aliquots rejected due to poor recycling ratios were preheated at high (280 or 300 °C) temperatures. This pattern may be caused by non-

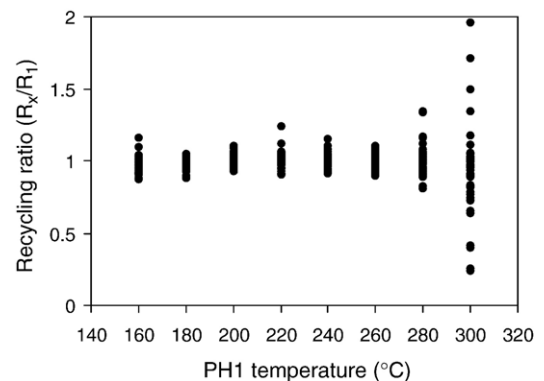


Fig. 4. Recycling ratio versus PH1 temperature for all the aliquots measured in this study ($n=652$). This ratio is calculated as R_x/R_1 where $R_1=L_1/T_1$ (the sensitivity-corrected luminescence intensity for the first regenerated dose) and $R_x=L_x/T_x$ (the sensitivity-corrected luminescence intensity of the repeated regenerated dose).

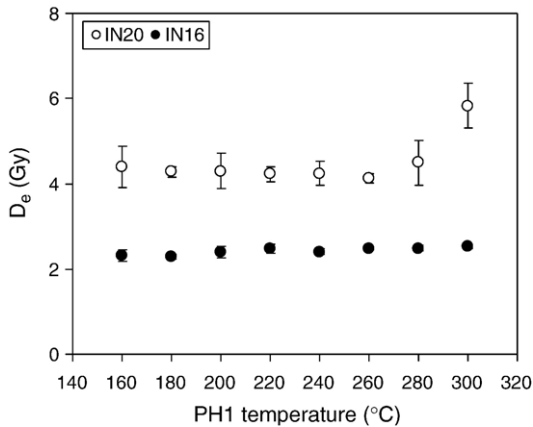


Fig. 5. D_e versus PH1 temperature for selected samples: IN20 (○) and IN16 (●). Each point is the mean value for three aliquots.

reproducible PH1 times leading to differential thermal erosion of the OSL signal. In addition, for most samples no systematic variation in D_e with preheat (PH1) temperature was observed (e.g. IN16 in Fig. 5); however, for some young (Holocene) samples the equivalent dose obtained using 280 and 300 °C PH1 temperatures is higher than those for preheat temperatures in the range 160 to 260 °C (e.g. IN20 in Fig. 5). This effect is interpreted as being due to thermal transfer and the D_e for samples such as IN20 was calculated using only aliquots preheated in the range 160 to 260 °C. Dose recovery experiments were performed on a selection of samples and results for two samples are shown in Fig. 6. The doses given in these experiments were chosen to be close to the measured D_e for each sample. The data indicate that the measurement procedure employed in this study is able to recover laboratory doses.

3. Results

3.1. Dose–response curves

All dose–response curves were fitted using the combination of a saturating exponential and a linear function as given in the caption to Fig. 7. A small number of aliquots yielded natural L_x/T_x values greater than the saturation value of the dose–response curve (Armitage et al., 2000) and for these aliquots no D_e could be calculated. With the exception of IN4, only one or two aliquots per sample were rejected on these grounds. For IN4, 8 of the 24 aliquots showed this property, and consequently the equivalent dose for this sample is regarded as a minimum. The phenomenon thought to give rise to such behaviour has been

investigated elsewhere (Bailey, 2004; Bailey et al., 2005). The errors on individual aliquot D_e values were based on photon-counting statistics, curve fitting error and included a 1.5% systematic measurement error (see Appendix 6.1 of Armitage, 2003). The OSL signals are generally very large, and hence the error on the D_e values for individual aliquots is dominated by the 1.5% systematic error.

3.2. Equivalent dose distributions

In this study equivalent dose distributions have been displayed as probability density functions (PDFs) with individual aliquot D_e values superimposed in ranked order. In the PDF each equivalent dose is represented as a Gaussian of equal area, whose height is inversely related to uncertainty. Similar plots have been published for aeolian sand samples from elsewhere in the world (e.g. Jacobs et al., 2003; Bray and Stokes, 2004; Stokes et al., 2004).

For most of the younger ($D_e < 30$ Gy) samples from Inhaca (e.g. IN12, IN14, IN15, IN16, IN18 and IN20), the aliquots resulted in a tight D_e distribution as shown in Fig. 8a for IN15. This gives rise to a mean D_e value of

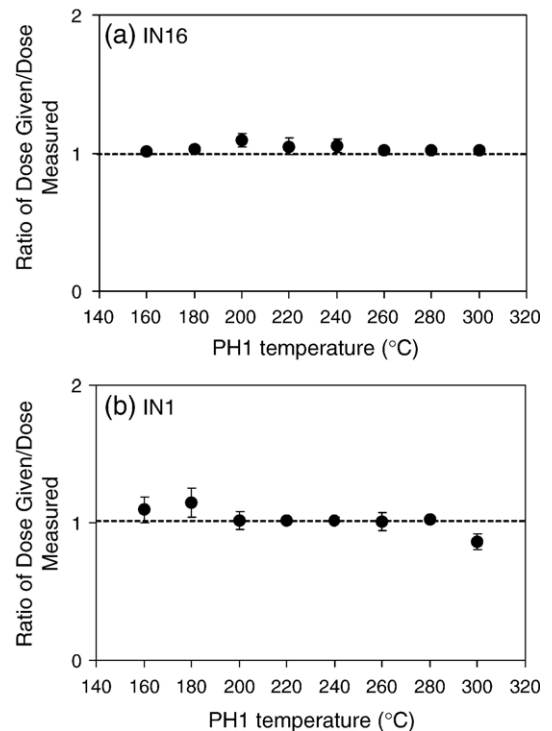


Fig. 6. Ratios for dose recovery versus PH1 temperature for experiments performed on (a) IN16 and (b) IN1 using known doses of 2.5 Gy and 99.2 Gy respectively. Each point is the mean value for three aliquots.

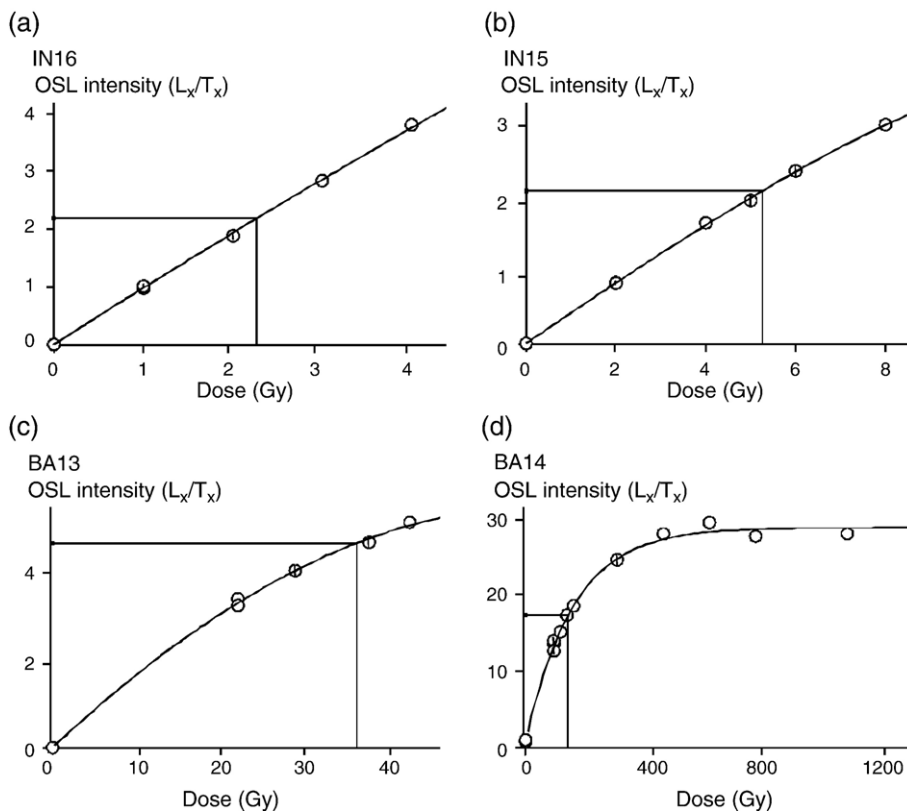


Fig. 7. Dose–response curves for selected samples: (a) IN16, (b) IN15, (c) BA13 and (d) BA14. The curves were fitted with a combined saturating exponential and linear function of the form $I(D) = I_1(1 - e^{-D/D_0}) + I_2D$, where $I(D)$ is the normalized OSL intensity (L_x/T_x).

5.2 ± 0.2 Gy. Even for a modern beach sand from the north-eastern tip of Inhaca (IN22) there is a tight distribution with only a few outliers (Fig. 8b). This gives rise to a mean D_e value of 0.006 ± 0.004 Gy, indicating that this sand was uniformly well-bleached by sunlight, and would result in an apparent age of no more than 10 years (using a typical dose rate of 1 Gy/ka). A tight distribution was also obtained for IN9, taken from the surface of a tidal flat on the western shore of Inhaca; in this case the mean D_e value (0.060 ± 0.005 Gy) was somewhat higher, but would have given an apparent age of no more than 65 years.

These low D_e values for modern samples and the tight distributions for the older samples are to be expected for well-bleached aeolian sands, and are similar to those published for sands of similar age (e.g. Bray and Stokes, 2004; Stokes et al., 2004; Singarayer et al., 2005). The results for the Inhaca samples provide confidence in the ages ranging from 2.1 ± 0.1 ka (IN16) to 22.2 ± 1.3 ka (IN12) (Table 1). For these samples, mean equivalent doses were calculated for each sample together with the associated standard error (σ/\sqrt{n} , where n is the number of D_e values

determined for a sample). However, for two samples in this age group (IN19 and IN21) tight D_e distributions were not obtained (e.g. Fig. 8c for IN21) and they are very different from the D_e distributions for IN15 (Fig. 8a), IN16 and IN18, despite the fact that all five samples were taken from geomorphologically similar parabolic dunes. For samples yielding wide dose distributions, both the mean (with associated standard error) and range of equivalent doses have been given in Table 1.

For the older samples (IN1, IN3, IN4 and IN11) taken as blocks from cliff faces, a range of D_e values was obtained, as exemplified in Fig. 8d (IN1). For these samples the D_e values obtained were close to twice the D_0 value for the saturating exponential function used to fit the growth curve (see caption to Fig. 7). This may have resulted in the large uncertainties on individual equivalent dose estimates, as well as broadening of the distributions, although these effects were not observed in the dose recovery data set for IN1 (Fig. 6b). Murray and Funder (2003) showed theoretically that broad distributions resulting from the curvature of the growth curve would be asymmetric and that the mean value of

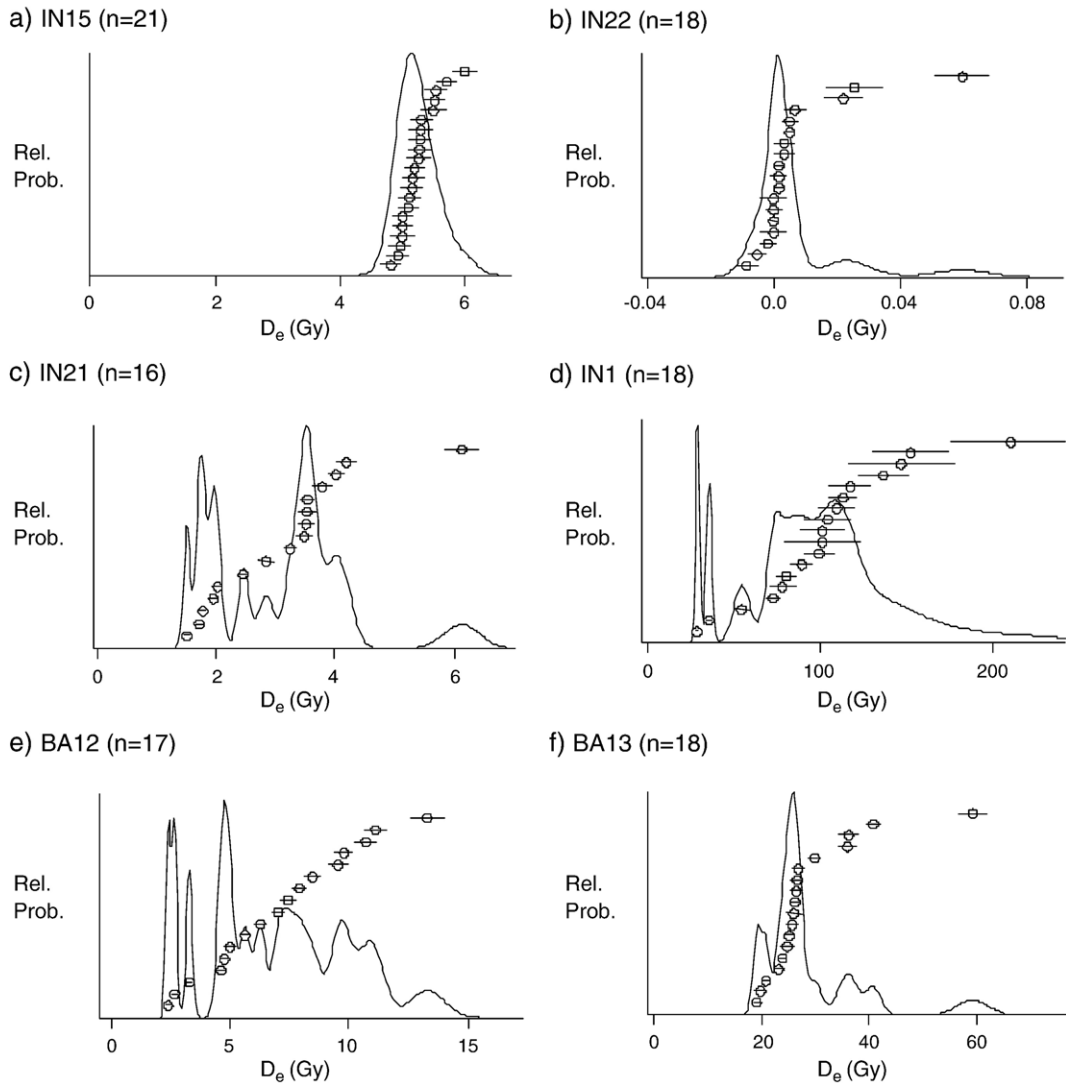


Fig. 8. D_e distributions shown as probability density functions and with individual D_e values shown with error bars in order of increasing value.

the distribution would be somewhat lower than the true palaeodose. They concluded that the median of the dose distribution was more likely to give an accurate estimate of the equivalent dose. The median value has been used to provide the age for samples with equivalent doses greater than 100 Gy (Table 1).

For Bazaruto, wide dose distributions were obtained for most samples (except for BA2, BA4 and BA13). Despite this, a modern beach sand (BA5) from the northern tip of Bazaruto gave a tight D_e distribution with a mean value of 0.003 ± 0.010 Gy, corresponding to an age of no more than 13 years. In addition, some aliquots of samples BA1 and BA14 were also affected by the proximity of their signals to the saturation level of the signal. A typical broad distribution is shown for

sample BA12 (Fig. 8e), taken from the A-horizon of a palaeosol at the top of the cliff at Zengueleme Point (Fig. 9); a very similar distribution was found for sample BA11 taken from the sand above the palaeosol. The sand unit below this palaeosol, BA13, had a much tighter distribution with only a few outliers (Fig. 8f). The apparent double peak in the PDF for BA13 is the result of the very small uncertainty calculated for individual D_e values. These small uncertainties are largely due to the very high OSL signal per unit dose (sensitivity) observed for all samples measured in this study. For the samples from Bazaruto, mean equivalent doses with associated standard errors were calculated for all samples, except BA14 for which the median was calculated. The range of equivalent doses has also

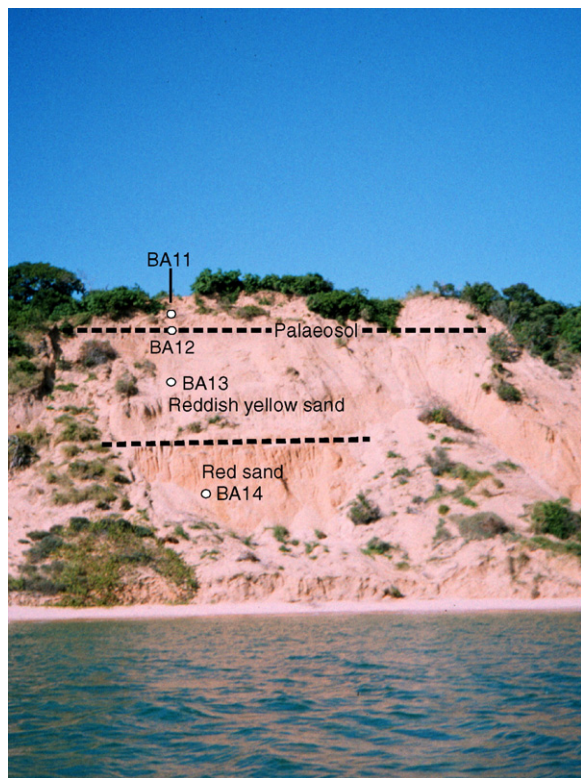


Fig. 9. Section at Zengueleme, Bazaruto.

been given for samples yielding broad distributions (Table 1).

3.3. Discussion of D_e distributions

Before moving to the interpretation of the OSL ages given in Table 1, it is necessary to comment on the D_e distributions obtained for the samples and compare them with those published by others. For a young (~ 5 ka) coastal dune from near Cape Agulhas, South Africa, Carr et al. (2006) presented a probability density function that was similar to that for IN15 (Fig. 8a). For an older (~ 70 ka) coastal dune at Wilderness, about 300 km east of Cape Agulhas, Bateman et al. (2004) reported a broad distribution of D_e values which could be explained by the range in D_e values obtained when they measured single quartz grains from the same sample. Broader than expected distributions were also found for three sands with ages of ~ 70 ka at Blombos on the southern Cape coast between Cape Agulhas and Wilderness (Jacobs et al., 2003). As in the current study, the results of a dose recovery experiment for one of the sands at Blombos showed that the value of a laboratory dose given to a laboratory bleached sample could be accurately and precisely recovered using the SAR protocol. Banerjee et

al. (2003), in their study of cemented coastal dune ridges with ages of ~ 60 or ~ 120 ka in south-eastern South Australia, also found D_e distributions that were broader than expected. They used the mean D_e value to calculate the OSL ages but could not provide a unique explanation for the range of values measured.

In order for such a large spread in D_e to be obtained for young sands (e.g. IN21, Fig. 8c, and BA12, Fig. 8e) for which the growth curves are linear, the most likely explanation is that some reworking has occurred, such that not all grains have been fully bleached. From Fig. 9, it can be seen that BA12 is taken from a palaeosol developed in the top of a reddish yellow weathered sand unit. Reworking of grains with a coloured surface (reducing light penetration) during soil formation would result in such a D_e distribution. Sample BA11, another sample with a wide D_e distribution, was collected from the overlying dune sand and from Fig. 9 it can be seen that the distribution might relate to recent mobilization of a thin layer of sand overlying the palaeosol.

For sample BA13 (~ 24 ka) the D_e distribution has only a few outliers. On the other hand, for older samples with doses of 100 Gy or higher, the broad D_e distributions could relate to the proximity of the L_N/T_N values of individual aliquots to the saturation level of the exponential component of the dose response curve. The exponential functions used typically have D_0 values of ~ 55 Gy, which would mean that for a dose of 110 Gy, the signal will be within 15% of the saturation value. For sample IN1, whose distribution is shown in Fig. 8d, the closeness to saturation could cause such scatter, even though the dose recovery test using 100 Gy (Fig. 6) showed perfect recovery. The scatter could result from a combination of the variable dose rate within a cemented dune containing the occasional heavy mineral grain and the relative contributions of the linear and exponential functions used to construct the dose response curve for each aliquot.

4. Geomorphological evolution

The geomorphological evolution of both Inhaca and Bazaruto islands shows a similar overall pattern which appears to be governed by sea-level highstands. The late Quaternary sea-level history of northern Mozambique has been outlined by Jaritz et al. (1977), although there is little published evidence from southern Mozambique. Sea-level curves for Southern Africa published by Ramsay (1995) and Ramsay and Cooper (2002) are in good agreement with the Jaritz et al. (1977) record, and indicate sea-level high-stands during MIS 7, 5e, 5c and the mid-Holocene. Inception of both islands probably

occurred with the formation of spits extending northwards from coastal promontories on the seaward side of river estuaries during a period of high sea-level (Hobday, 1977; Cooper and Pilkey, 2002). These spits have not been directly dated. However, sample IN4, which was collected from the planar cross-bedded aeolianite (Barreira Vermelha coastline) forming the core of the western dune cordon of Inhaca, yields a minimum age of 250 ka, suggesting formation in early MIS 7 or before. Bazaruto may also have begun to form at this time but no samples of this age were measured. The oldest sample from Bazaruto was deposited at the beginning of MIS 5 (BA14).

4.1. Evolution prior to MIS 2

Both islands experienced two phases of dune accretion during or immediately prior to MIS 5. The reddish yellow sand unit observed discontinuously along the western margin of Bazaruto was sampled from the ~20 m high bluff at Zengueleme, south of Ponta Gengarene (Figs. 3 and 9). The basal deposits of this aeolian sand succession accreted at 126 ± 12 ka (BA14) indicating deposition during high sea-level conditions early in MIS 5. A second, probably distinct, dune building phase is indicated by the formation of an aeolianite at Ponta Ganhala on the northeastern margin of Bazaruto at 88.8 ± 7.4 ka (BA1) (Fig. 3). On the northeastern point of Cabo Inhaca (Fig. 2) these two phases of island building are clearly distinct. The older (150 ± 24 ka, IN1) and younger (98.2 ± 16.0 ka, IN3) deposits exposed at Cabo Inhaca are separated by a rhizolith-rich unit (Fig. 10), indicating a hiatus in deposition and the formation of significant vegetation cover. A significant sand body was also deposited on the older western limb of Inhaca during MIS 5 (101 ± 8 ka, IN11).

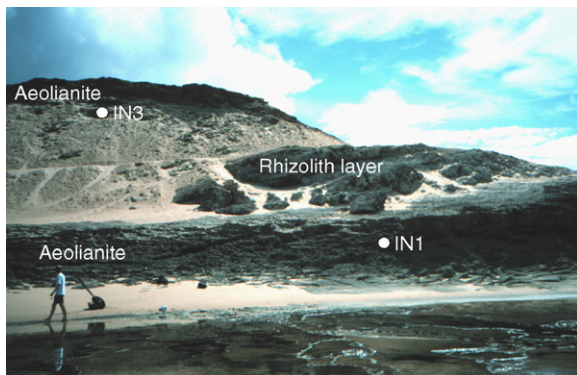


Fig. 10. Aeolianites separated by a rhizolith-rich layer at Cabo Inhaca.

No record of island-building has been found between the end of MIS 5 and c.25 ka. However, during the latter part of MIS 2 (23.8 ± 2.4 ka, BA13 and 22.2 ± 1.3 ka, IN12) both islands experienced accretion of dune systems represented by the reddish yellow weathered sand units which overlie reddened MIS 5 deposits. These sands accreted as prograding parabolic dunes and may represent reworking of the underlying material in response to decreased vegetation cover. The colour of these units could indicate inheritance of ferruginous coatings due to limited aeolian transportation of this sand following deflation from the reddened parent material. It is envisaged that vegetation cover was reduced at this time due to a regional lowering of the water table in response to the rapidly falling sea-levels during MIS 2 (Kocurek et al., 2001).

The global record of carbonate aeolianite deposition summarized by Brooke (2001), the detailed record of aeolianite/barrier dune construction in the southern Cape region of South Africa (Bateman et al., 2004; Carr et al., 2006), formation of aeolianite at Langebaan Lagoon on the Cape West Coast (Roberts and Berger, 1997), and the evidence for mid-Holocene accretion of the Maputaland coastal barrier dune (Wright et al., 2000), suggest that coastal dune accretion occurred during interglacial sea-level highstands. In general, the ages presented above support this conclusion, the single exception being IN1 (150 ± 24 ka) which falls within the MIS 6 sea-level lowstand. The OSL age for this sample is likely to be underestimated as, apart from the three smallest D_e values (Fig. 8d), the natural OSL signals are close to the saturation level obtained for laboratory OSL measurements. Several lines of geomorphological evidence also suggest that the 150 ka age is unlikely to be correct. First, Illenberger (1996) has argued that on the humid (600–900 mm rainfall per annum) southern Cape coastline, coastal dune activity is restricted to an area immediately adjacent to the beach, which is the only supply of unvegetated mobile sand. He suggested that during glacial regressions, humidity is high enough to allow rapid colonization by vegetation, and therefore stabilization, of exposed marine sediments. Consequently, dune deposits adjacent to the present-day coast must have formed during periods when the sea was close to its present-day level. Secondly, detailed investigations of the Maputaland continental shelf have revealed submerged barrier dunes formed during periods of lower sea-level (Ramsay, 1994). These dunes indicate that even during periods of glacial sea-level fall, the climate system is sufficiently humid to prevent significant landward migration of aeolian sediment. Finally, although small-scale remobilization of sediment appears

to have occurred during MIS 2, no large sand bodies from this period have been found on either island. For the above reasons, and in light of the ages presented above, we conclude that the dune cores on Inhaca and Bazaruto are primarily high sea-level deposits, and not formed in response to increased sediment supply during marine regressions as postulated by [Hobday \(1977\)](#). The two dune building phases prior to MIS 2 observed on both islands are tentatively correlated with MIS 5e and 5c though the uncertainties associated with the OSL ages preclude unequivocal assignment of deposits to specific marine isotope sub-stages.

4.2. Evolution since MIS 2

Both islands have been geomorphologically active since MIS 2, as was the Maputaland coastal plain where parabolic dunes formed from remobilization of older dunes ([Botha and Porat, 2000](#)). The early Holocene transgression swept sediment from the continental shelf landwards and eroded the unconsolidated dune deposits on the coast. This sediment was subsequently formed into parabolic dunes by the prevailing SE winds. These dunes prograded over the eastern and western dune ridges of Inhaca and are represented by parabolic dune limbs sampled on the west of the island (IN18, 14.3 ± 0.9 ka and IN14, 11.5 ± 0.7 ka). Subsequent flooding of the Saco da Inhaca embayment by the Holocene marine transgression cut off the sediment supply to the western side of Inhaca, preserving these dunes at the surface. Erosion of the eastern coast increased the sediment supply to the parabolic dunes which overrode the eastern limb of Inhaca throughout the Holocene. The lower topography in the centre of the island is probably due to the absence of a core of aeolianite or older dunes in this area. The northern margin of Inhaca consists of a large palaeo-tidal flat dated to 3.7 ± 0.2 ka (IN20). Since this age represents the final abandonment and, therefore, stabilization of the tidal flat, this feature was almost certainly formed during the mid-Holocene high sea-level event at c.5 ka identified by [Ramsay \(1995\)](#). The erosional event related to development of the palaeo-tidal flat truncated a large parabolic dune dated to 6.0 ± 0.3 ka (IN15) at the northeastern extremity of the supratidal flats. Parabolic dunes post-dating this event (IN16, 19, 21) override the palaeo-tidal flats, although a reliable age can only be obtained for IN16 (2.1 ± 0.1 ka). Based on the D_c distributions, the other two samples show evidence of reworking. The ages for IN15 and IN20 indicate that the mid-Holocene high sea-level period started after 6.0 ± 0.3 ka and had ended by 3.7 ± 0.2 ka, providing independent age control for this event.

Limited parabolic dune formation occurs on Inhaca at present since beachrocks and aeolianites protect the eastern coastline from erosion and thick vegetation covers much of the island.

The evolution of Bazaruto since MIS 2 is very similar to that of Inhaca. The interior dunes on Bazaruto were probably formed during the early Holocene transgression when significant quantities of sediment were liberated from the continental shelf. During the early to mid-Holocene the eastern shoreline of Bazaruto appears to have stabilized with the formation of a north–south-oriented fringe of beachrocks, dated at its northern tip to 7.2 ± 0.9 ka (BA2). However, south of Ponta Govane these beachrocks now form reefs off the coast, suggesting a significant landward retreat of the southern Bazaruto coastline ([Cooper, 1991](#)). Sediment was transported inland as narrow, extended parabolic dunes deriving from the foredunes on the eastern coast of Bazaruto. These dunes accreted to form a complex coastal barrier during the late Holocene. Relatively recent shoreline retreat and stabilization is indicated by the presence of a 1.0 ± 0.1 ka beachrock (BA8) at Ponta Govane. Unlike Inhaca, the vegetation on Bazaruto is relatively sparse and significant erosion of the eastern coast is occurring, as indicated by extensive active dune systems along the entire eastern coastline of Bazaruto. Together with the significant landward retreat of the coastline south of Ponta Govane, this suggests that Bazaruto is far less stable than Inhaca and may suffer further erosion.

5. A model for the evolution of barrier islands on the Mozambique coast

The data presented above allow the formulation of a generalized model for the formation of barrier islands along the Mozambique coast. This may be summarized as:

- 1) Initial formation of a spit constructed by longshore currents and possible aeolian accretion, extending downdrift from a headland of older aeolianite or a structural offset ([Hobday, 1977](#); [Cooper and Pilkey, 2002](#));
- 2) Formation of large coast-parallel sand bodies composed of material eroded from the continental shelf during marine transgressions, possibly as early as MIS 7 or before. These sand bodies are stabilized by vegetation and the formation of aeolianites and beachrocks. Successive transgressions, especially during MIS 5, may form composite islands with several phases of deposition superimposed on one another;

- 3) Limited localized reactivation of the surface of older sand bodies during low sea-level events in response to reduced vegetation cover caused by lowering of the regional water-table. Contrary to the expectation of several workers (e.g. [Hobday, 1977](#); [Cooper and Pilkey, 2002](#)), no significant quantities of sediment are supplied to either island during sea-level low-stands or regressions; and
- 4) The early Holocene transgression sweeps significant quantities of sediment onshore to be formed into foredune complexes that supply sand to ascending parabolic dune systems. The early Holocene shoreline may be stabilized by beachrock. Continuing erosion of the islands' oceanic margin supplies sediment for further parabolic dune and spit formation. This erosion may result in the formation of parabolic dunes which migrate into the interior of the island. It is likely that similar reworking of sediment occurred whenever sea-level stabilized at its modern level.

Although this model specifically applies to barrier islands, it is likely that the regionally extensive dune complex of the Mozambican and Maputaland coastal plains was affected by changes in sea-level in a similar manner. It is interesting to note that [Cooper and Pilkey \(2002\)](#) ascribe the height of the eastern limb of Inhaca to continuous deposition throughout each glacial–interglacial cycle regardless of sea-level. The data from Inhaca and Bazaruto do not support this assertion. It is possible that the great height of the dunes along the Maputaland coast, the eastern ridge of Inhaca included, is due to their longevity, allowing repeated phases of accretion onto a stabilized core with each successive transgression. If this is the case, the early formation of extensive beachrock and aeolianite plays a major role in the geomorphic evolution of this coastline by protecting the coastal dunes.

Acknowledgements

This work was undertaken while SJA was in receipt of an Aberystwyth Postgraduate Research Studentship to study for a PhD in the Institute of Geography and Earth Sciences, University of Wales Aberystwyth. This manuscript was greatly improved by the constructive comments of two anonymous referees.

References

[Achimo, M., Mugabe, J., Cuamba, F., Haldorsen, S., 2004.](#) Late Weichselian to Holocene evolution of the Maputo Bay, Mozambique. In: [Momade, F., Achimo, M., Haldorsen, S. \(Eds.\)](#), *The*

- Impact of Sea-level Change, Past, Present, Future: Boletim Geológica*, vol. 43, pp. 20–27.
- [Adamiec, G., Aitken, M.J., 1998.](#) Dose rate conversion factors: update. *Ancient TL* 16, 37–49.
- [Armitage, S.J., 2003.](#) Testing and application of luminescence techniques using sediment from the southeast African coast. Unpublished PhD thesis, University of Wales Aberystwyth.
- [Armitage, S.J., Bailey, R.M., 2005.](#) The measured dependence of laboratory beta dose rates on sample grain size. *Radiation Measurements* 39, 123–127.
- [Armitage, S.J., Duller, G.A.T., Wintle, A.G., 2000.](#) Quartz from southern Africa: sensitivity changes as a result of thermal pretreatment. *Radiation Measurements* 32, 571–577.
- [Atkins, J.E., McBride, E.F., 1992.](#) Porosity and packing of Holocene river, dune and beach sands. *Bulletin of the American Association of Petroleum Geologists* 76, 339–355.
- [Bailey, R.M., 2004.](#) Paper I—simulation of dose absorption in quartz over geological timescales and its implications for precision and accuracy of optical dating. *Radiation Measurements* 38, 299–310.
- [Bailey, R.M., Armitage, S.J., Stokes, S., 2005.](#) An investigation of pulsed-irradiation regeneration of quartz OSL and its implications for the precision and accuracy of optical dating (Paper II). *Radiation Measurements* 39, 347–359.
- [Ballarini, M., Wallinga, J., Murray, A.S., van Heteren, S., Oost, A.P., Bos, A.J.J., van Eijk, C.W.E., 2003.](#) Optical dating of young coastal dunes on a decadal time scale. *Quaternary Science Reviews* 22, 1011–1017.
- [Banerjee, D., Hildebrand, A.N., Murray-Wallace, C.V., Bourman, R.P., Brooke, B.P., Blair, M., 2003.](#) New quartz SAR-OSL ages from the stranded beach dune sequence in south-east South Australia. *Quaternary Science Reviews* 22, 1019–1025.
- [Barbouthi, A.I., Rastin, B.C., 1983.](#) A study of the absolute intensity of muons at sea level and under various thicknesses of absorber. *Journal of Physics. G, Nuclear and Particle Physics* 9, 1577–1595.
- [Bateman, M.D., Holmes, P.J., Carr, A.S., Horton, B.P., Jaiswal, M.K., 2004.](#) Aeolianite and barrier dune construction spanning the last two glacial–interglacial cycles from the southern Cape coast, South Africa. *Quaternary Science Reviews* 23, 1681–1698.
- [Berger, G.W., Murray, A.S., Havholm, K.G., 2003.](#) Photonic dating of Holocene back-barrier coastal dunes, northern North Carolina, USA. *Quaternary Science Reviews* 22, 1043–1050.
- [Botha, G.A., Porat, N., 2000.](#) Dune system remobilisation on the Maputaland coastal plain, South Africa, during the Late Pleistocene and Holocene. *Quaternary International* 63/64, 29–30.
- [Botha, G.A., Bristow, C.S., Porat, N., Duller, G.A.T., Armitage, S.J., Roberts, H.M., Clarke, B.M., Kota, M.W., Schoeman, P., 2003.](#) Evidence for dune reactivation from GPR profiles on the Maputaland coastal plain, South Africa. In: [Bristow, C.S., Jol, H.M. \(Eds.\)](#), *Ground Penetrating Radar in Sediments: Special Publication—Geological Society of London*, vol. 211, pp. 29–46.
- [Botter-Jensen, L., Mejdahl, V., 1988.](#) Assessment of beta dose-rate using a GM multicounter system. *Nuclear Tracks and Radiation Measurements* 14, 187–191.
- [Botter-Jensen, L., Bulur, E., Duller, G.A.T., Murray, A.S., 2000.](#) Advances in luminescence instrument systems. *Radiation Measurements* 32, 523–528.
- [Bray, H.E., Stokes, S., 2004.](#) Temporal patterns of arid–humid transitions in the south-eastern Arabian Peninsula based on optical dating. *Geomorphology* 59, 271–280.
- [Brooke, B., 2001.](#) The distribution of carbonate eolianite. *Earth-Science Reviews* 55, 135–164.

- Carr, A.S., Thomas, D.S.G., Bateman, M.D., 2006. Climatic and sea level controls on Late Quaternary eolian activity on the Agulhas Plain, South Africa. *Quaternary Research* 65, 252–263.
- Cooper, J.A.G., 1991. Beachrock formation in low latitudes: implications for coastal evolutionary models. *Marine Geology* 98, 145–154.
- Cooper, J.A.G., Pilkey, O.H., 2002. The barrier islands of Southern Mozambique. *Journal of Coastal Research* 36, 164–172.
- Duller, G.A.T., 1996. The age of the Koputaroa dunes, southwest North Island, New Zealand. *Palaeogeography, Palaeoclimatology, Palaeoecology* 121, 105–114.
- Duller, G.A.T., 2003. Distinguishing quartz and feldspar in single grain luminescence measurements. *Radiation Measurements* 37, 161–165.
- Duller, G.A.T., 2004. Luminescence dating of Quaternary sediments: recent advances. *Journal of Quaternary Science* 19, 183–192.
- Duller, G.A.T., Bøtter-Jensen, L., Murray, A.S., 2000. Optical dating of single sand-sized grains of quartz: sources of variability. *Radiation Measurements* 32, 453–457.
- Dutton, T.P., 1990. A conservation master plan for sustained development of the Bazaruto Archipelago. World Wide Fund for Nature (WWF), Southern African Nature Foundation (SANF) and Oceanographic Research Institute (ORI).
- Flemming, B.W., 1981. Factors controlling shelf sediment dispersal along the southeast African continental margin. *Marine Geology* 42, 259–277.
- Flores, G., 1973. The Cretaceous and Tertiary sedimentary basins of Mozambique and Zululand. In: Blant, G. (Ed.), *Sedimentary Basins of the African Coasts: 2nd part*, Assoc. Afr. Geol. Surv., Paris, pp. 81–111.
- Förster, R., 1975. The geological history of the sedimentary basin of southern Mozambique, and some aspects of the origin of the Mozambique Channel. *Palaeogeography, Palaeoclimatology, Palaeoecology* 17, 267–287.
- Hobday, D.K., 1977. Late Quaternary sedimentary history of Inhaca Island, Mozambique. *Transactions of the Geological Society of South Africa* 80, 183–191.
- Hong, D.G., 1998. Luminescence stimulated from quartz by green light: developments relevant to dating. Unpublished PhD thesis, University of Edinburgh.
- Illenberger, W.K., 1996. The geomorphic evolution of the Wilderness dune cordons, South Africa. *Quaternary International* 33, 11–20.
- Jacobs, Z., Wintle, A.G., Duller, G.A.T., 2003. Optical dating of dune sand from Blombos Cave, South Africa: I. Multiple grain data. *Journal of Human Evolution* 44, 599–612.
- Jaritz, W., Rüder, J., Schlenker, B., 1977. Das Quartär im Küstengebiet von Moçambique und seine Schwermineralführung. *Geologisches Jahrbuch*, vol. B26, pp. 3–93. Hannover.
- Kocurek, G., Robinson, N.I., Sharp, J.M., 2001. The response of the water table in coastal aeolian systems to changes in sea level. *Sedimentary Geology* 139, 1–13.
- Maud, R.R., Botha, G.A., 2000. Deposits of the south eastern and southern coasts. In: Partridge, T.C., Maud, R.R. (Eds.), *The Cenozoic of Southern Africa: Oxford Monographs on Geology and Geophysics*, vol. 40, pp. 19–32.
- Miller, W.R., 2001. The bathymetry, sedimentology and seismic stratigraphy of Lake Sibaya — northern KwaZulu-Natal. *Bulletin*, vol. 131. Council for Geoscience.
- Muacanhia, T., 2004. Environmental changes on Inhaca Island, Mozambique: development versus degradation. In: Momade, F., Achimo, M., Haldorsen, S. (Eds.), *The Impact of Sea-level Change, Past, Present, Future: Boletim Geológica*, vol. 43, pp. 28–33.
- Murray, A.S., Funder, S., 2003. Optically stimulated luminescence dating of a Danish Eemian coastal marine deposit: a test of accuracy. *Quaternary Science Reviews* 22, 1177–1183.
- Murray, A.S., Olley, J.M., 2002. Precision and accuracy in the optically stimulated luminescence dating of sedimentary quartz: a status review. *Geochronometria* 21, 1–16.
- Murray, A.S., Wintle, A.G., 2000. Luminescence dating of quartz using an improved single-aliquot regenerative-dose protocol. *Radiation Measurements* 32, 57–73.
- Prescott, J.R., Hutton, J.T., 1988. Cosmic ray and gamma ray dosimetry for TL and ESR. *Nuclear Tracks and Radiation Measurements* 14, 223–227.
- Ramsay, P.J., 1994. Marine geology of the Sodwana Bay shelf, southeast Africa. *Marine Geology* 120, 225–247.
- Ramsay, P.J., 1995. 9000 years of sea-level change along the southern African coastline. *Quaternary International* 31, 71–75.
- Ramsay, P.J., Cooper, J.A.G., 2002. Late Quaternary sea-level change in South Africa. *Quaternary Research* 57, 82–90.
- Roberts, D., Berger, L.R., 1997. Last Interglacial (c. 117 kyr) human footprints from South Africa. *South African Journal of Science* 93, 349–350.
- Singarayer, J.S., Bailey, R.M., Ward, S., Stokes, S., 2005. Assessing the completeness of optical resetting of quartz OSL in the natural environment. *Radiation Measurements* 40, 13–25.
- Stokes, S., Bailey, R.M., Fedoroff, N., O'Marah, K.E., 2004. Optical dating of aeolian dynamism on the West African Sahelian margin. *Geomorphology* 59, 281–291.
- Wright, C.I., 2002. Aspects of the Cenozoic evolution of the northern KwaZulu-Natal coastal plain, South Africa. *Bulletin*, vol. 132. Council for Geoscience.
- Wright, C.I., Miller, W.R., Cooper, J.A.G., 2000. The late Cenozoic evolution of coastal water bodies in Northern KwaZulu-Natal, South Africa. *Marine Geology* 167, 207–229.